RSC Advances

REVIEW

View Article Online
View Journal | View Issue

Cite this: *RSC Adv.*, 2022, **12**, 14137

Research progress and applications of silica-based aerogels – a bibliometric analysis

Chao Ji,†[ab] Shuang Zhu,†[bc] Enshuang Zhang,[d] Wenjing Li,[d] Yuanyuan Liu,[d] Wanlin Zhang,[d] Chunjian Su,*[a] Zhanjun Gu *[bc] and Hao Zhang*[d]

Silica aerogels are three-dimensional porous materials that were initially produced in 1931. During the past nearly 90 years, silica aerogels have been applied extensively in many fields. In order to grasp the progress of silica-based aerogels, we utilize bibliometrics and visualization methods to analyze the research hotspots and the application of this important field. Firstly, we collect all the publications on silica-based aerogels and then analyze their research trends and performances by a bibliometric method regarding publication year/citation, country/institute, journals, and keywords. Following this, the major research hotspots of this area with a focus on synthesis, mechanical property regulation, and the applications for thermal insulation, adsorption, and Cherenkov detector radiators are identified and reviewed. Finally, current challenges and directions in the future regarding silica-based aerogels are also proposed.

Received 8th March 2022
Accepted 2nd May 2022

DOI: 10.1039/d2ra01511k

rsc.li/rsc-advances

1. Introduction

Aerogels are a kind of three-dimensional porous material with more than 90% porosity,[1] and are often obtained by a sol–gel process,[2] fiber accumulation,[3,4] or 3D printing.[5] Owing to the characteristics of low density and high specific surface area,[6] aerogels have been applied in many fields such as thermal insulation,[7–9] wastewater treatment,[10,11] acoustic insulation,[12,13] and drug delivery.[14,15] At present, the value of aerogels in blanket and granular form in the global market is estimated at €250 Mio per year, with an annual growth rate as high as ~20%.[16] Within all kinds of aerogels, silica-based aerogels (SAs) have become the most commonly used aerogels. Initially, SAs consist of necklace-like particles which are synthesized through the sol–gel method.[17,18] It was firstly introduced by Kistler in 1931 when he used gas to replace the liquid of wet gels to get silica aerogels.[19] SAs have not been extensively studied over the next several decades, on account of the complex and time-consuming procedure. It was not until Teichner and Nicoloan produced silica aerogels in 1972, using tetramethyl orthosilicate (TMOS) as a precursor, was the SA produced in a continuous process and obtained through the sol–gel process.[20] After the appearance of different technologies, the synthetic process has become diversified. With the introduction of freeze casting and spinning technologies, stacked fibers formed SAs in 2014, and they possess a stronger compressible ability by the transformation of major pores and the densification of minor pores.[21–23] Recently, with the development of three-dimensional (3D) printing technology, the combination of 3D printing technology and chemical synthesis provides a new method for the synthesis of SAs in 2020,[24] which can manufacture structurally complex products by the design of 3D models and then improve their adaptability in different occasions.[25–27] In addition to the above methods, SAs are also produced by deposition on the other aerogels.[28] As the most commonly used aerogels, SAs exhibit high-temperature resistance (>800 °C),[29,30] low density,[31,32] and low thermal conductivity,[33] which make them widely used in both civil and military fields. In the military fields, SAs are used to capture hypervelocity particles and protect the primary battery pack of the Alpha Particle X-ray Spectrometer from the influence of low temperatures.[34,35] Similarly, SAs are also used as Cherenkov detector radiators to identify the particles.[36] In the civil fields, SAs have been used in the insulating bricks, glass fillers,[37,38] and adsorption of CO_2 and harmful substances.[39–42]

Owing to the wide exploration and applications of SAs, it is difficult to grasp the research progress of SAs. Thus, we employ the bibliometric analysis method to analyze a large body of SA-related literature, with an aim to obtain their research trend and hotspots. In this study, we first obtain all the research papers in the field of SAs from Web of Science (WoS) Core Collection and identify the publication trends, most contributive countries/

[a]*College of Mechanical and Electronic Engineering, Shandong University of Science and Technology, Qingdao 266590, China. E-mail: suchunjian2008@163.com*

[b]*Key Laboratory for Biomedical Effects of Nanomaterials and Nanosafety and CAS Center for Excellence in Nanoscience, Institute of High Energy Physics and National Center for Nanoscience and Technology of China, Chinese Academy of Sciences, Beijing 100049, China. E-mail: zjgu@ihep.ac.cn*

[c]*Center of Materials Science and Optoelectronics Engineering, College of Materials Science and Optoelectronic Technology, University of Chinese Academy of Sciences, Beijing 100049, China*

[d]*Aerospace Institute of Advanced Material & Processing Technology, Beijing 100074, P. R. China. E-mail: ruizhangh@163.com*

† These authors contributed equally to this work.

regions, institutions, and journals. Meanwhile, research hotspots and main application fields of SAs are also discussed. Specifically, the synthesis of SAs, mechanical property regulation, and their application for thermal insulation, adsorption, and Cherenkov detector radiator are the main research fields. At the end of this review, current challenges and the promising future direction regarding this popular field are also proposed. This study provides a novel strategy to present the research advances and also introduces comprehensive design methods of SAs for different fields, which may serve as a reference review and also accelerate the development of this field.

2. General bibliometrics in terms of publication year, country/institution, and research area

2.1 Data collection and processing method

Bibliometric analysis is a method of analyzing big data based on a large number of documents.[43,44] It can depict the publication trend, contributing countries/regions and institutions, and hotspots, which can endow us with a more comprehensive analysis of SAs.[45–47] In detail, the data in this study are searched by the search strings of "ts = (SiO_2 or silica or "silicon dioxide") and ts = (aerogel* or xerogel* or cryogel*) not ts = ("silica template*")" until 12th February 2022 from the WoS Core Collection databases. It is worth noting that aerogels that are studied by us represent gel networks whose liquid was replaced by air. However, they are sometimes named as aerogels, cryogels, and xerogels according to different drying methods: supercritical drying, freeze-drying, and ambient pressure drying (APD), respectively.[48,49] Because they all represent the same kind of structure, we search all of their names to represent all gel structures filled with air. In total, there are 151 publications published discontinuously for more than fifty years before 1900, we here only analyzed data after 1900 to reflect the connection between publications and time. A total of 9071 publications are found, with 7937 articles, 268 reviews, 127 meeting abstracts, and other types of publications. Since some document types, such as meeting abstracts and letters, are not frequently cited material, we utilize only articles and reviews in our following analysis.[50] In addition, to acquire the application for SAs in many fields, we acquire the research hotspots with the assistance of keywords co-occurrence analysis by Vosviewer. We merge repetitive keywords including their singular and plural forms (*i.e.*, aerogel and aerogels) and their different names, such as SiO_2, silica, and silicon dioxide, using thesaurus files.[51,52]

2.2. Publication trend and contributing countries/regions and institutions

Fig. 1a shows the annual publications and citations from 1990 to 2021. During this period, the number of publications increases as time goes on. Meanwhile, the number of citations also shows an increasing trend year by year. This trend indicates the growing attention among the scientific community to SAs. Owing to their wide application potential, many countries/regions pay efforts on SAs. Hence, the twelve most contributive countries/regions are listed, which are sorted according to the number of total publications (Fig. 1b). China is the most contributive country with 1950 publications. Following are the USA (1497 publications) and France (745 publications). Meanwhile, the index of h represents h publications that were each cited at least h times.[53] Thus, the h-index is introduced to reflect the citation performance.[54] USA, China, and France exhibit higher h-index, which indicates the publications received higher attention. What's more, from the perspective of institutions, the Chinese Academy of Sciences, with 215 publications, contributes the highest number of publications (Fig. 1c). University of Montpellier 2 (42 h-index) and Université Claude Bernard Lyon 1 (45.92 average citations) have the highest h-index and average citations, respectively.

2.3 Bibliographic coupling analysis of referenced sources

Bibliographic coupling analysis of referenced sources could not only identify the most contributive journals but also provide the preliminary information of SAs simply according to the journal names and related-area of journals. As shown in Fig. 2a, the three journals including Journal of Non-Crystalline Solids, Journal of Sol–Gel Science and Technology, and Microporous and Mesoporous Materials receive many SA-related publications. In addition, with the assistance of the identified journals, we could obtain the preliminary information of SAs. For instance, Journal of Non-Crystalline Solids and Ceramics

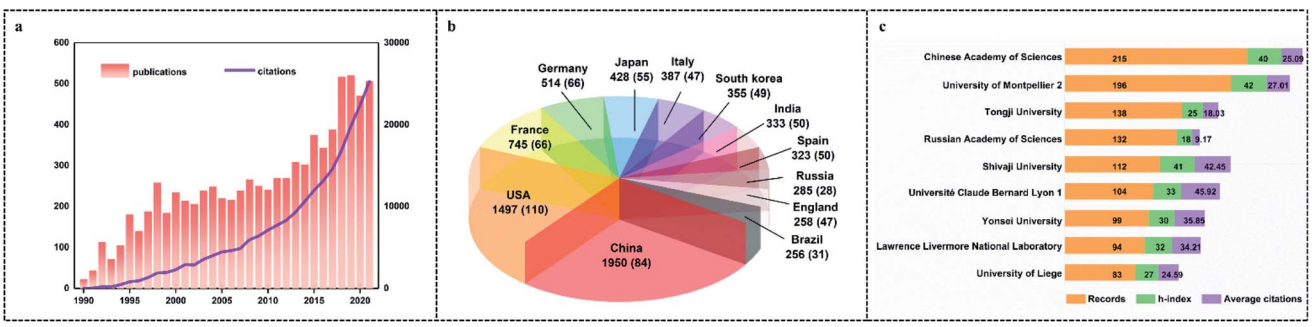

Fig. 1 (a) The trend of publications and citations. (b) The most contributive countries/regions based on the total publication. H-index values appear in the brackets. (c) The most productive institutions based on the total publication.

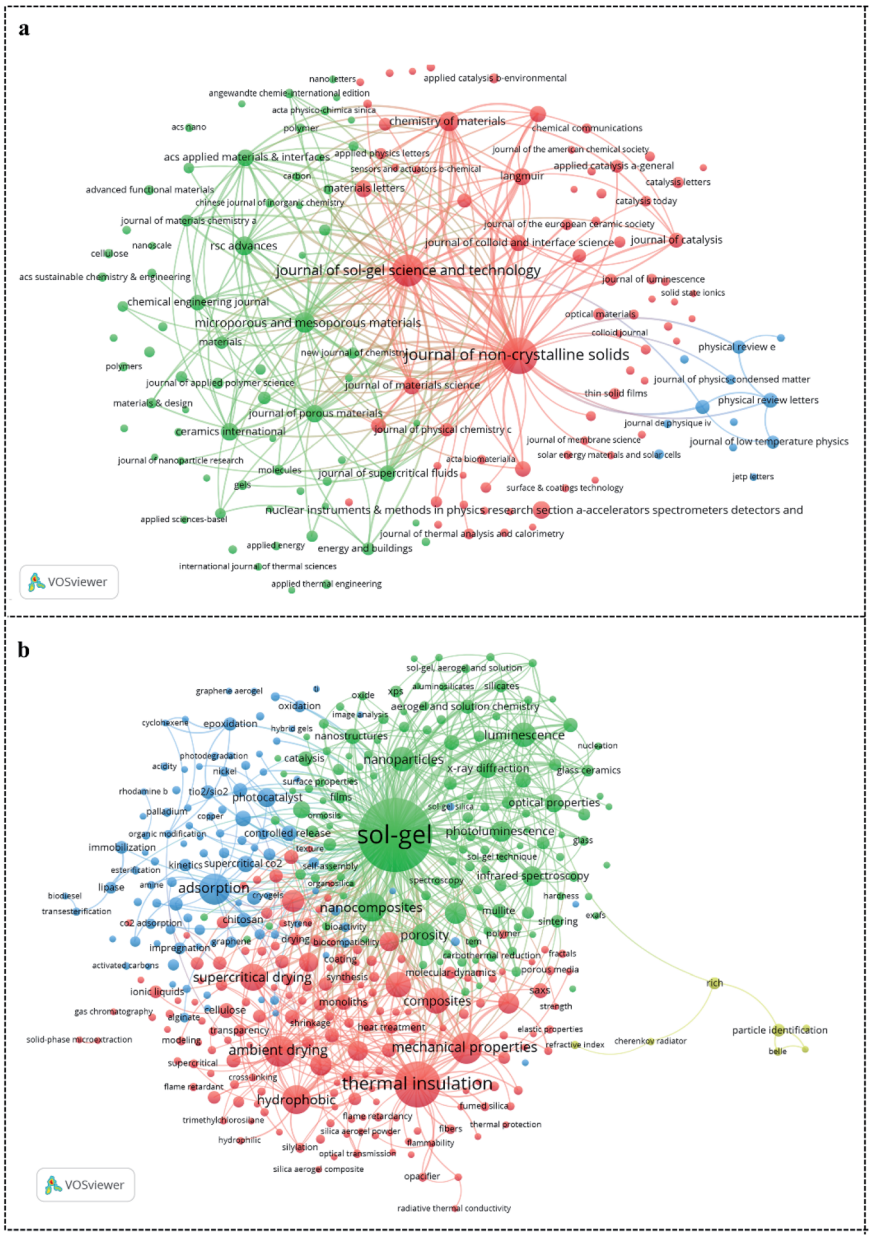

Fig. 2 (a) Bibliographic coupling analysis of referenced sources. The node size represents the number of publications. (b) Keyword co-occurrence analysis with at least 10 occurrences. The node size represents the occurrence frequency of the keywords.

International shows the characteristics of silica such as non-crystal materials and composition of ceramics. Journal of Sol–Gel Science and Technology indicates that they are commonly synthesized by the sol–gel method. Microporous and Mesoporous Materials and Journal of Porous Materials demonstrate their high porosity. Nuclear Instruments Methods in Physics Research Section A: Accelerators, Spectrometers, Detectors and Associated Equipment shows that SAs can be used as Cherenkov detector radiators.

2.4. Keyword co-occurrence analysis

After obtaining the general bibliometric information of SAs research, we further utilize keyword co-occurrence analysis to acquire research hotspots of SAs. “Aerogel”, “silica”, “aerogels”, and “silica aerogels”, as the most frequent keywords, but they fail to reveal useful information about SAs. Thus, we remove them from the network to highlight the other keywords.[55] Fig. 2b shows the 409 items of keywords co-occurrence analysis (threshold = 10). The larger a circle is, the more frequently a keyword occurs. In addition, Vosviewer is also able to classify keywords into different clusters with different colors, and each cluster presents a similar research field.[56] In our dataset, all keywords are divided into four clusters. Specifically, keywords in the green cluster are mainly related to the synthesis and characterization. Keywords in the red cluster are connected with mechanical capacity and thermal insulation. Meanwhile, the blue and yellow clusters mainly reflect the adsorption ability

and Cherenkov detector radiator, respectively. Such keywords reveal that the main research hotspots of SAs focus on synthesis, mechanical capacity regulation, and their applications for thermal insulation, adsorption, and Cherenkov detector radiator. In the next section, we will give a brief introduction of each research hotspot of SAs according to our analys.

3. Synthesis technologies

Sol–gel, as a kind of synthesis method of SAs, is the biggest node in the keyword network, which indicates that the synthesis of SAs is the most popular research topic. Consequently, we here summarize different synthesis technologies according to their appearance time (Fig. 3). Here, SAs can be divided into three categories according to different synthesis technologies for different shapes: particulate silica-based aerogels (PSAs), fibrous silica-based aerogels (FSAs), and 3D printing SAs. Initially, SAs consist of necklace-like particles through the sol–gel method and they are named as PSAs.[59] Afterward, with the introduction of freeze casting and spinning technologies, stacked fibers were used to form FSAs.[60] FSAs have lamellar macrostructure or cellular macrostructure. Recently, 3D printing technology can manufacture structurally complex 3D printing SAs by the design of 3D models.[61] Although 3D printing SAs have a similar microstructure to PSAs, the macrostructure of 3D printing SAs can be controllably designed.

3.1 PSAs

PSAs are composed of necklace-like silica particles. They are obtained through three steps, respectively are silica wet gels synthesis, aging/modification, and drying.[62] Silica wet gels are obtained by the sol–gel method which transforms liquid precursors into a sol to a gel by hydrolysis and condensation reaction.[63,64] In the hydrolysis and condensation reaction, primary particles are formed first and then agglomerated into secondary particles. Finally, secondary particles crosslink each other into silica particle networks.[65] The silica particle networks and the liquid in the interstices formed silica wet gels. Generally, precursors could be silicates[66,67] or silicon alkoxides.[57,64,68–71] To accelerate the process of hydrolysis and condensation, different acid or base catalysts were added.[72–74]

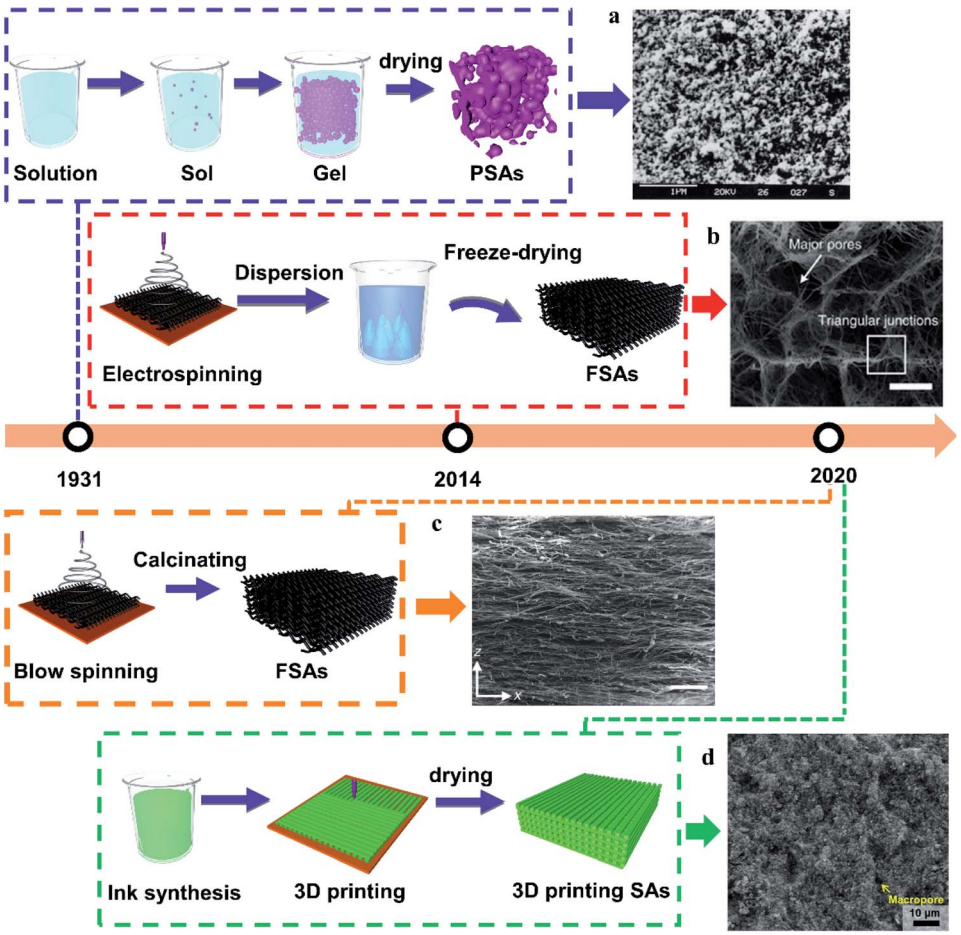

Fig. 3 (a) The representative microscopic image of PSAs Copyright 1999, Elsevier.[57] (b) The representative microscopic image of FSAs obtained by ice template method the scale represents 20 μm. Copyright 2020, Springer Nature.[21] (c) The representative microscopic image of FSAs obtained by solution blow spinning method. The scale rerepresents 500 μm. Copyright 2020, Springer Nature.[22] (d) The representative microscopic image of 3D printing SAs. Copyright 2021, American Chemical Society.[58]

There are many research discussions and summaries regarding the sol–gel process,[75–77] so we will not repeat it here.

Aging is a process that precursors continue hydrolysis and condensation,[78] which is achieved through the following two processes. One is that silica of particle surface is dissolved and deposited on the necks of gel networks. Another is that small particle is dissolved and precipitated into big particle.[79] Both of these processes can increase the strength of the networks and reduce shrinkage and breakage in the subsequent phases. Thus, prolonging aging time or raising the aging temperature can improve the strength and rigidity of the solid skeleton of SAs. Many studies reported that the aging effect depends on the temperature, solvent, concentration, and aging time.[80–82] With the increase of time, temperature, and concentration, the process of aging speeds up. Moreover, the rational selection of solvents is also significant to the aging effect.[83] For example, Omranpour *et al.*[84] discussed the aging effect in different solvents. The compressive modulus of aerogels, aging in *N*-hexane, increased 2 and 4 times compared with methanol and water, respectively. Significantly, methanol can inhibit the condensation reaction, which results in a weak effect.

Drying is a process to remove the solvent in silica wet gels, which includes three main methods: APD, freeze-drying, and supercritical drying.[85] APD is a drying process under ambient pressure. The wet gels are suffered from capillary stresses because APD is achieved by the transition from liquid to gas phase.[86] Because of the capillary stresses during solvent evaporation, SAs obtained by APD were more likely to shrink and break than other drying methods. The capillary stress (P_r) is as follows: $P_r = (2\gamma \cos \theta)/r$, where γ is the surface tension of the solution, θ is the contact angle between the solution and the pore wall, and r represents the radius of the pore. Therefore, to minimize shrinkage and breakage, there are three methods to minimize capillary stress. The first method is to exchange the solution of the wet gels with a lower surface tension solution.[87,88] The second method is to modify the wet gels with hydrophobic functional groups which endow the gel networks higher contact angle (θ).[89,90] Mutual repulsion produced by hydrophobic functional groups can maintain the structural integrity during the process of drying, different from the shrinkage of SAs with hydrophilic functional groups.[91–93] For example, Wei *et al.*[33] modified silica aerogels with the hydrophobic group in low surface tension solvent. The as-prepared aerogels have a crack-free structure and volume shrinkage of less than 1%. The third method is to prolong aging time, which endows gel networks with stronger skeletons to withstand capillary stress.[94] Next, during the process of freeze-drying, the ice crystals arise from the solution in the wet gels below the freezing point and then are rapidly sublimed under low pressure.[95,96] Because of the sublimation process without liquid–gas transition, the wet gels do not suffer from capillary stresses.[97] But Scherer *et al.*[98] mentioned that the development of ice crystals can destroy the wet gels in his study, which is easy to cause shrinkage and breakage. Some strategies (such as aging) can increase the strength of the wet gels and then minimize the risk of shrinkage and breakage. Lastly, supercritical drying, which is achieved above the critical point of the solvent by controlling the temperature and pressure, is a drying method that absents the interface between the liquid and the gas phase.[99] During the process of supercritical drying, the liquid and the gas phase become a homogeneous supercritical phase, which can avoid capillary stresses.[100] However, the drawbacks of supercritical drying are not negligible such as high cost and strict instrument specification.[101]

3.2 FSAs

FSAs are composed of stacked silica fibers by the ice template or solution blow spinning method.[22,102] In terms of the ice template method, it includes three steps: the acquisition and dispersion of silica fibers, freeze casting, and freeze-drying. First, silica fibers which usually are obtained by electrospinning are dispersed.[103] To obtain homogeneous structure silica fibers skeletons, silica fibers should be uniformly dispersed in silica sol during the process of freeze casting.[104,105] Then, silica fiber skeletons are obtained by the freeze casting process. In this process, owing to the solvent solidifying below freezing point, silica fibers in solution are rejected by ice crystals and then stack each other to form silica fiber skeletons.[106,107] Finally, after freeze-drying, the solidified solvent is replaced by air and stacked silica fibers become FSAs. The development condition of ice crystals influences the characteristics of the porosity because the porosity is obtained by the removal of ice crystals porosity. Many studies show that the freezing rate, solvents, additives, and the growth direction of the ice crystals can regulate the morphology of the porosity by influencing the growth of ice crystals.[108] It should be noted that the nucleation rate is higher than the crystal growth rate at a low ice solidification rate. It finally results in large ice crystals at a low ice solidification rate, because large ice crystals grow at the cost of smaller ice crystals.[109] Conversely, nucleation rate is higher than the ice crystal growth rate faster ice solidification rate at a high ice solidification rate, which can result in small pores and regular structure. For example, Gutiérrez *et al.*[110] obtained aerogels with smaller pore sizes by increasing the freezing rate. Additionally, additives can change the morphology by regulating the growth of ice crystals.[111–115] For example, Xian *et al.*[114] prepared aerogels with 30 μm pore size, adding 20 wt% glycerol, while the pore size of aerogels without glycerol was 20–50 μm. It is worth noting that different solvents have been used to produce different types of pore morphologies during the freeze casting of scaffolds and porous ceramics.[116,117] For example, Deville *et al.*[118] obtained lamellar pore morphologies during freeze casting in water, while Araki *et al.*[119] produced dendritic pore morphologies during freeze casting in camphor-naphthalene. However, research on the solvent influence for FSAs is still inadequate. Meanwhile, the cellular can be changed by controlling the growth direction of the ice crystals. For example, Si *et al.*[120] prepared FSAs with isotropic cellular structures after unidirectional freezing, while Su *et al.*[23] produced FSAs with anisotropic cellular structures after directional freezing. Different from the PSAs which exhibit weak connections between the particles, the FSAs illustrate stronger compressible ability, which is caused by the transformation of

major pores and the densification of minor pores.[21] Meanwhile, this phenomenon is also reflected in the relation between relative Young's modulus and relative density. The relative Young's modulus is proportional to relative density to the power of $n((E/E_s) \sim (\rho/\rho_s)^n)$, where ρ and ρ_s represent the density of the aerogels and the bulk solid materials, while E and E_s reveal their Young's modulus. The cellular structure produced by freeze-drying is similar to the structure of wood or honeycomb. This biomimetic structure provides a cellular-dominated mechanical behavior $((E/E_s) \sim (\rho/\rho_s)^2)$, such as open-cell cellular foams.[122,123] Such structure can also endow FSAs with negative Poisson's ratio caused by reversion of the fibrous layer,[124] which can bear more stress.[125] However, PSAs illustrate inefficient stress transfer among random particulate structures $((E/E_s) \sim (\rho/\rho_s)^3)$.[126] For example, Si *et al.*[120] prepared ceramic nanofibrous aerogels (CNFAs). They obtained silica fibers by electrospinning of silica sol. Silica fibers were homogenized with polyacrylamide solution to become a uniformly dispersed solution. And silica fibers in aluminoborosilicates (AlBSi) and polyacrylamide solution were freeze casting and freeze-drying to obtain composite pre-aerogels (CPAs). After calcined at 900 °C, the adjacent silica fibers of CPAs were connected by AlBSi glass ceramics and then CNFAs were obtained. The stress–strain curve showed that CNFAs can carry the weight over 7000 times of themselves without fracture, and they exhibited 12% plastic deformation loading of 60% compressive strain after 500th cycles. Compared with FSAs with hard bonding points obtained by calcination under high-temperature, FSAs with elastic bonding exhibit stronger compressibility. For example, Wang *et al.*[121] prepared silica nanofibrous (SNF) aerogels which are similar to the juncus pith structure (Fig. 4a). They obtained silica fibers by electrospinning of silica sol. Then the silica fibers were dispersed in hydrolyzed silane sol. The dispersion of the fiber was poured into the model, experiencing freeze casting, and freeze-drying to become silica nanofibrous aerogels. The hydrolyzed silane sol could crosslink with the surface of the fibers to form the Si–O–Si crosslinking networks without high sintering. More importantly, hydrolyzed silane sols with different hydroxyl groups, such as TEOS, MTMS, and DMDMS, have been investigated as crosslinkers (Fig. 4b). The mechanical property measurement showed that SNF/MTMS aerogels did not exhibit plastic deformation, while SNF/TEOS and SNF/DMDMS aerogels exhibited 2% and 10% plastic deformation loading of 50% compressive strain after 5th cycles, respectively (Fig. 4c). It means that the elastic resilience depends on crosslinking degree and flexibility of crosslinkers.

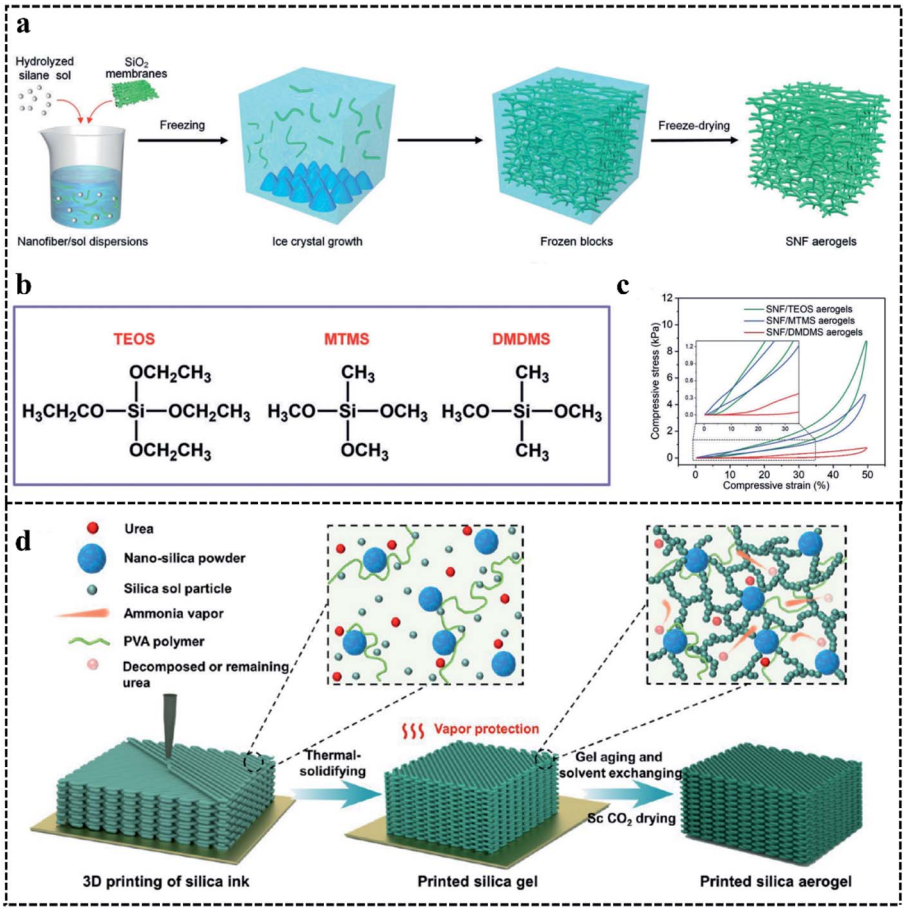

Fig. 4 (a) Synthetic route of SNF aerogels. (b) Structures of different crosslinking silane coupling agents. (c) Compressive σ *versus* ε at the 5th loading–unloading cycle of different SNF aerogels.[121] Copyright 2020, John Wiley and Sons. (d) Synthetic route of thermal-solidifying SAs.[58] Copyright 2021, American Chemical Society.

The solution blow spinning is also used to produce FSAs. During the process of solution blow spinning, the inner chamber and the outer chamber connect with silica sol and blow, respectively.[127,128] FSAs with a layered structure can be directly produced under pressure drop between the inner chamber and the outer chamber. For example, Jia *et al.*[22] prepared lamellar ceramic aerogels. They obtained Al_2O_3–SiO_2 aerogels by solution blow spinning of alumina-silica sol and calcinating. After adding $AlCl_3$ to the precursor solution, the prepared fibers are easily and stably accumulated into aerogels with lamellar structure rather than random fiber distribution. It could cause Al_2O_3–SiO_2 aerogels to be completely restored to their original shape while the SiO_2 aerogels have weak poor compressibility loading of 80% compressive strain along in the direction perpendicular to the stacked layers. The fibers became denser when pressure was loaded and the fibers were rejected by lap joints when pressure was released, which endowed the Al_2O_3–SiO_2 aerogels with high compressibility.

3.3 3D printing SAs

3D printing is an additive manufacturing technique, which deposits materials layer by layer, with the help of computer-aided design technology.[24,129,130] Different from the traditional chemical synthesis technologies, 3D printing can manufacture structurally complex products by the design of 3D models. It avoids weak processability and enlarges the application fields of prepared products. 3D printing, especially direct ink writing (DIW),[25–27,58,131] are used to produce SAs through three steps: ink synthesis, 3D printing, and drying. DIW needs inks that are non-Newtonian fluids, whose viscosity decreases with the shear rate increases.[132,133] In order to obtain SAs, the liquid of 3D printed gels needs to be removed by APD, freeze-drying, or supercritical drying, as discussed above. Zhao *et al.*[25] first prepared pure 3D printing SAs by DIW. They used silica aerogel particles and PPGNH as thickeners to increase viscosity and dispersibility. Ammonia vapor could accelerate the sol–gel process transformation, achieving the solidification of 3D-printing objects. After supercritical drying, 3D printing SAs with high mesoporosity can be implemented. Meanwhile, 3D printing SAs were directly used to protect equipment from overheating. Other solidification methods are proposed because solidification implemented by ammonia vapor is difficult to achieve scale production. For example, Wang *et al.*[58] proposed thermal-solidifying SAs by DIW (Fig. 4d). The ink consisted of PVA solution, urea, silica sol, glycerol, and nanosilica particles. After printing, the thermal solidification of 3D-printing objects was achieved by warming. The hydrogen bond cross-linking effect between PVA and nanosilica powders can regulate rheological properties and form self-supporting structures. The addition of glycerol with a high boiling point and low capillary pressure also avoids the cracks and shrinkage caused by volatilization. The thermal solidification was achieved through the hydrolysis of urea. The hydrolysate of urea is alkaline in solution, which could accelerate sol–gel progress. Finally, 3D printing SAs with abundant mesopores were produced after supercritical drying. In addition to this, freeze casting, as a solidification method, has been used in the process of other aerogels. For example, Kam *et al.*[134] fabricated cellulose nanocrystals aerogels which were solidified by freeze casting. Xyloglucan was a binder and controlled the rheology. During the process of 3D printing, the material was extruded on a cold platform to achieve solidification by freeze casting. In order to simultaneously conduct printing and freeze casting, the temperature was manually controlled to ensure that two top layers were unfrozen and others frozen. Although freeze casting has not been used in the solidification of SAs, combining freeze casting and a more intelligent temperature control system has the potential to become a scale production method. Meanwhile, with the assistance of freeze casting, Newtonian inks can be used to prepare aerogels.[135] For example, Yan *et al.*[5] prepared Ag nanowire aerogels using inkjet printing, which were solidified by freeze casting solution. After low viscous Ag nanowire suspension was deposited on the cold plate whose temperature was −30 °C, the suspension was frozen layer by layer and eventually formed aerogels.

4. Mechanical property regulation

The mechanical property is the second-largest node in the red cluster of the keyword network, which indicates that the mechanical property regulation of SAs, especially PSAs, plays an important part in the process of machining. Because the pure PSAs are composed of necklace-like silica particles. The connection points between silica are Si–O–Si bondings which are stiffbonds.[65,136] It means that their connection between particles is weak and pure PSAs are fragile materials. When forces act on it, pure PSAs tend to crack, which was adverse to subsequent processing, limiting their applications.[137] However, FSAs possess the stronger compressible ability which is achieved by the transformation of major pores and the densification of minor pores.[138] Similarly, 3D printing SAs are produced according to designed 3D models, which avoids subsequent processing after manufacture and decreases the possibility of cracking.[25] Thus, to make the best of SAs, improving their mechanical property is indispensable. The strategies are listed as follows: cross-linking and adding reinforcing phases.

4.1 Cross-linking

Another strategy is cross-linking with polymers which could form extra chemical bonds between silica particles.[139] For example, Jiang *et al.*[140] added triethoxysilane-grafted polyrotaxane in the hydrolyzed TEOS sols to obtain wet gels. The drying process was achieved by supercritical drying. With the increase of triethoxysilane-grafted polyrotaxane content, the gelling time became shorter. This phenomenon illustrated that polyrotaxane chains can cross-link silica particles and form a "pearl-necklace-type" structure. This structure resulted in 2 orders of magnitude compression strength compared with pure SAs. It was worth noting that prepared SAs showed the same porosity as pure SAs. In another study, Meador *et al.*[141] prepared epoxy crosslinked SAs. TMOS and (aminopropyl)triethoxysilane (APTES) were chosen as the precursors of wet gels. Epoxy cross-

linkers with different numbers of functional epoxide could crosslink with the amines on the surface of silica. The mechanical test suggested that the stress at breakpoint and modulus of as-prepared SAs which were cross-linked with different numbers of functional epoxide both increase by as much as 2 orders of magnitude. It should be noted that the SAs cross-linked with trifunctional epoxide exhibited the strongest stress at breakpoint and modulus. The cause of the phenomenon is that as the number of epoxy groups increases, the molecules may become too constrained to increase reactive sites.

4.2 Adding reinforcing phases

Adding reinforcing phases can disperse and divert the external forces over the entire SAs to reinforcing phases, which is also an effective strategy to enhance the robustness of SAs.[142] Owing to the high toughness or compressibility of carbon nanotubes (CNT),[143] graphenes, fibers,[144] and polymer skeleton,[71] they are often used as reinforcing phases. For example, He *et al.*[145] prepared bacterial cellulose aerogels/silica aerogels. The dispersed bacterial cellulose fibers formed a three-dimensional skeleton *via* freeze-casting and were impregnated to silica sols under vacuum. With the hydrolysis and condensation of silica sols, the silica aerogels gradually formed as fillers. The bacterial cellulose aerogels/silica aerogels could bear a compressive strain up to 80% and recover to their original volume after the release of the stress. More importantly, the maximum stress was 25.6 kPa at 50% strain and no significant decrease in maximum stress at 50 cyclic compressions. In another study, Lamy-Mendes *et al.*[143] prepared CNT-silica aerogels composites. HNO_3 was for the first time used to form oxygen functional groups on CNT, which is easy to modify with Methyltrimethoxysilane (MTOS) on CNT. The hexadecyltrimethylammonium bromide which can disperse CNT in base solution and control the microstructure of the silica aerogels and MTOS-CNT were added to the solvent. Then Methyltrimethoxysilane (MTMS) and (3-aminopropyl)trimethoxysilane (APTMS), as the precursors, were added into the solvent, which formed silica networks under acid and basic catalyst. The CNT-silica aerogels composites were obtained after aging and APD. The uniaxial compression measurement showed the addition of CNT increased the hardness of CNT-silica aerogels. Meanwhile, Young's modulus increased when CNT or/and APTMS were added, suggesting the reinforcing effect of reinforcing phases.

5. Applications of SAs

5.1 Thermal insulation

Thermal insulation is the biggest node in the red cluster and the second-largest node in the keyword network, indicating that SAs have a low total thermal conductivity and are mainly used for thermal insulation. Because of the small porosity of SAs (<4 mm), convection heat transfer is ignorable.[146] Thus, the total thermal conductivity (λ_{toal}) of SAs is composed of solid heat transfer (k_{solid}), air heat transfer (k_{gas}), and radiation heat transfer (k_r).[147] The total thermal conductivity is as follows: $\lambda_{toal} = k_{solid} + k_{gas} + k_r$. Owing to the low density and porosity of SAs, SAs have the potential to be thermal insulation materials. At the same time, the application of SAs in thermal insulation gradually expands from the military field to the civil field. For example, for the first time since 1997, SAs were firstly used as insulators on the Mars Rover, as a part of the Pathfinder mission to protect the primary battery pack of the Alpha Particle X-ray Spectrometer from the influence of low temperatures.[148] In addition, SAs are used as thermal insulation coating for space suits.[149] With the development of SAs, they were applied in civil fields such as a building. For example, Wernerywe *et al.*[38] prepared an aerogels-filled insulating brick. The thermal conductivity of them decreased by 35%, compared with commercially perlite filling brick. It means that we can use thinner insulating bricks to achieve high thermal insulation, which could greatly improve building usage space. Furthermore, based on the promising potential of SAs in the thermal insulation field, many methods were developed to further decrease the thermal conductivity of SAs. Next, we discuss the strategies for reducing thermal conductivity by regulating solid heat transfer, air heat transfer, and radiation heat transfer.

Solid heat transfer is a way to transfer heat through the solid network. During the process of solid heat transfer, heat transfer is realized in the form of free electrons and phonons.[150] For silica, the phonons heat transfer is the main way in solid heat transfer and is achieved by forceful lattice vibration and the transmission between adjacent units.[151,152] The interface between gas and solid generates strong boundary scatterings, which can effectively inhibit the transfer of phonons and then reduce the solid heat transfer.[153] This process can be achieved by regulating structure.[23] For example, Jia *et al.*[22] prepared lamellar ceramic aerogels. The air within and between stacked layers can effectively decrease solid heat transfer in the direction perpendicular to the stacked layers. And owing to the tortuous and convoluted solid networks, solid heat transfer was limited. Compared with the thermal conductivity in the direction perpendicular to the stacked layers, the Al_2O_3–SiO_2 aerogels had lower thermal conductivity as low as 0.034 Wm^{-1} K^{-1} in the direction parallel to the stacked layers (Fig. 5a–c). Therefore, we can adjust the structure of SAs to obtain anisotropic materials with extremely low thermal conductivity in a certain direction.

Air heat transfer is a way to transfer heat through the collision of air molecules with each other and the solid networks.[154] Because the mean free path of air molecules is 70 nm under ambient conditions, the air heat transfer is constant when the pore size of SAs is more than 70 nm. When the pore size is below 70 nm, the air heat transfer is restricted according to the Knudsen effect.[155,156] Thus, it is an effective method to suppress air heat transfer by reducing the pore size of SAs (Fig. 5d).[157] For example, Dou *et al.*[158] prepared binary-network structured silica aerogels. The silica fibers obtained by electrospinning were dispersed in a hydrolyzed silane sol for freeze casting and freeze-drying. After calcined at 700 °C, silica fibrous aerogels were obtained. The prepared silica fibrous aerogels were immersed into MTMS-based silica sol. During the hydrolysis and condensation reaction, the binary-network gels could be

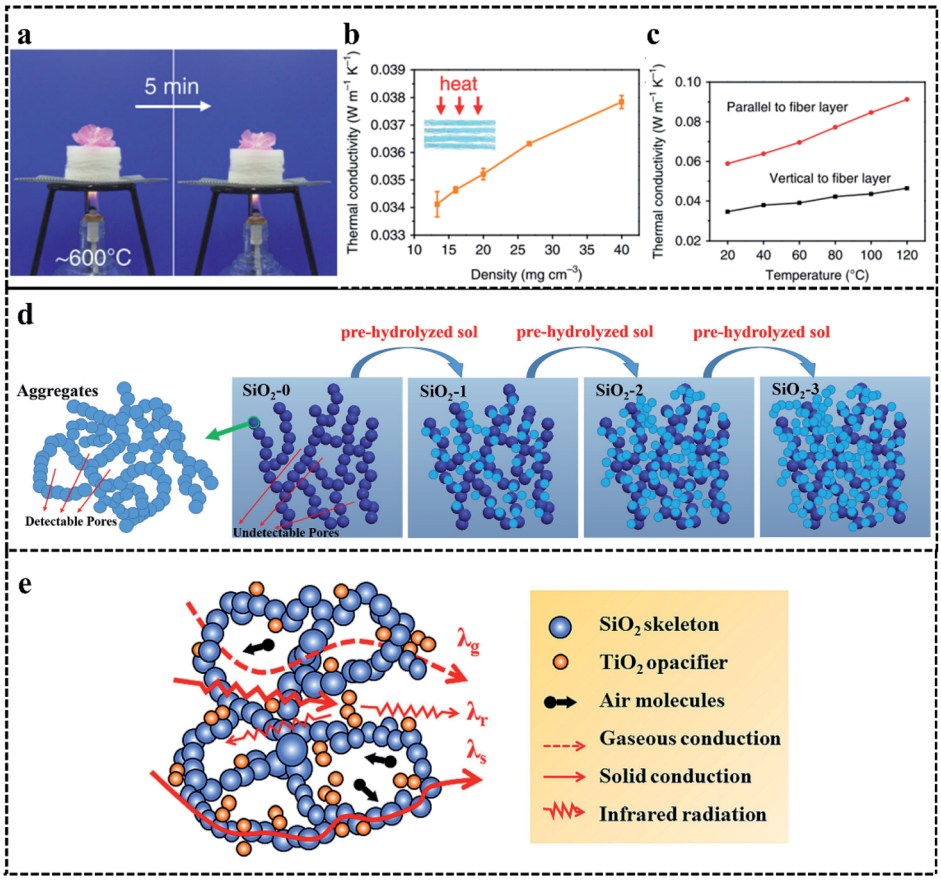

Fig. 5 (a) The thermal insulation performance of Al_2O_3–SiO_2 aerogels at high temperature. (b) The thermal conductivity of Al_2O_3–SiO_2 aerogels at different densities. (c) The thermal conductivity of the Al_2O_3–SiO_2 aerogels with a density of 16 mg cm^{-3}.[22] Copyright 2020, Springer Nature. (d) The inhibition of air heat transfer by decreasing pore size.[157] Copyright 2017, Elsevier. (e) The mechanism of adding opacifier for inhibiting thermal insulation.[159] Copyright 2021, Elsevier.

formed. Finally, binary-network structured silica aerogels were obtained after the APD and calcination at 800 °C. The thermal conductivity test showed when the mass of MTMS increased to 0.5 g, the thermal conductivity decreased to 21.96 mWm^{-1} K^{-1} at ambient temperature, while thermal conductivity without adding of MTMS is more than 25 mWm^{-1} K^{-1}. This phenomenon is caused by the average pore size change from 34.22 nm to 3.41 nm, with the content of MTMS increased to 0.5 g. The decrease of average pore size limits the collisions of gas molecules, which effectively decreased thermal conductivity by suppressing air heat transfer. However, when the content of MTMS increases to 2 g, the thermal conductivity is more than 26 mWm^{-1} K^{-1}. This is related to the higher solid heat transfer caused by greater bulk density, despite the small pore size (6.09 nm). As a result, the proper content of silica sol can inhibit the thermal conductivity by suppressing air heat transfer.

Radiation heat transfer is a way to transfer heat through electromagnetic waves, which exist in the form of infrared radiation.[160] However, pure SAs are transparent in the infrared wavelength range between 3 and 8 μm.[161] Meanwhile, radiation heat transfer will increase as the temperature grows. Therefore, adding opacifiers with high infrared radiation scattering or absorption ability (such as TiO_2,[159] graphene,[162] and Y_2O_3 (ref. 163)) can effectively reduce the radiation heat transfer to inhibit thermal conductivity (Fig. 5e). For example, Zhu *et al.*[162] prepared graphene-doped silica aerogels. They added graphene into hydrolyzed silica sol and then added a base catalyst to form graphene-doped silica wet gels. After the aging and supercritical drying, graphene-doped silica aerogels were obtained. The thermal conductivity test showed the thermal conductivity decreased from 0.030 to 0.0184 Wm^{-1} K^{-1}, with the increase of the content of graphene from 0 to 0.10 wt%, at ambient temperature. This was caused by the uniform dispersion of graphene in silica aerogels, which reduced radiation heat transfer and had no contribution to the solid heat transfer. When the content of graphene continues to increase to 0.15 wt%, the thermal conductivity increased to 0.0191 Wm^{-1} K^{-1}. A mass of graphene connected each other, which made a greater impact on solid heat transfer than radiation heat transfer. Thus, the thermal conductivity can be controlled by adding opacifiers.

5.2 Adsorption

The blue cluster in the keyword network shows the application of SAs for adsorption. The adsorption is the most frequent keyword in the blue cluster, which reflects the common feature

of these applications. Other keywords such as copper, rhodamine B, and CO_2 adsorption illustrated the adsorption for heavy metal ions, oil and organic dyes, and CO_2. As a global issue, water pollution is a health risk due to its damage to humans and the environment. Heavy metal ions in water pollution can damage the liver, kidneys and even cause cancer.[164] Thus, taking proper strategy to remove heavy metal ions in water pollution is indispensable. The SAs possess small pores and large surface areas, which can provide a mass of adsorption sites.[165,166] Meanwhile, they are easily surface modified to meet different needs for adsorption.[167] These characteristics are in favor of adsorption and make them available in wastewater treatment. In general, the process of adsorption is related to electrostatic interactions, hydrogen bonds, or chelate effects.[175] The effect of adsorption for heavy metal ions was influenced by (1) pH, (2) temperature, (3) time, (4) type of ions, (5) initial concentration of ions, (6) the content of SAs, and (7) surface functionalization.[176,177] At the different pH, the surface charges of aerogels are influenced. With the increase of pH, a stronger adsorption ability was exhibited, which can attribute to the more negative surface charge on aerogels. In general, the adsorption effect of heavy metal ions is proportional to temperature. The rapid diffusion of heavy metal ions at a high temperature promotes the adsorption effect. However, a lower temperature favor adsorption when the process of adsorption is an exothermal reaction. The heavy metal ions are gradually adsorbed along with time, until reach equilibrium. The rate of adsorption gradually decreases, because of more available adsorption sites at the beginning. Same aerogels produce different effects on the different types of ions, which can attribute to the different interactions between functional groups and ions. The higher the initial concentration of ions, the higher the adsorption efficiency. With the increase of the content of SAs, more heavy metal ions are removed, due to a mass of available exchangeable sites caused by the high surface area. Surface functionalization of silica aerogels can enhance the chelate effect for heavy metal ions (such as sulfhydryl,[171,178] carboxyl,[179] and amino group[180,181]). Different surface-modified SAs adsorbents and their adsorption condition of heavy metal ions are summarized in Table 1.

Besides heavy metal ions, oil and organic dyes in water pollution also raise considerable concerns. Hydrophobic and hydrophilic modification on the surface of SAs have been used to oil and organic dyes adsorption, respectively.[182–186] For example, Chen *et al.*[187] prepared hydroxyl modified SAs to adsorb Congo red (CR) and Methyl blue (MB) (Fig. 6a). The pH_{PZC} of hydroxyl modified SAs was 5.8. When the pH of the solution was higher than 5.8, the negative charges on the surface of them promoted MB adsorption. When the pH of the solution was lower than 5.8, the positive charges on the surface promoted the CR adsorption. Thus, the removal rate of MB and CR are both more than 90% at pH 9 and 4, respectively. This is because MB and CR are cationic and anionic dyes, respectively. Meanwhile, hydrophobic SAs can easily be infiltrated by oil with low surface tension values, which is in favor of adsorption for oil. For example, Selay *et al.*[189] prepared different surface-

Table 1 Different surface-modified SAs adsorbents and their adsorption condition. R: range, O: optimum, E: equilibrium

Functionalization	Heavy metal ions	The initial concentration of ions	pH	Time	The content of SAs	Temperature	Ref.
Mercaptopropyl trimethoxysilane (MPTMS)	Cd^{2+}	R 50–400 mg mL^{-1}	R 2–7	R 10–60 min	R 0.02–0.12 g		168
		O 50 mg mL^{-1}	O 6	E 30 min	O 0.05 g		
	Pb^{2+}	R 50–400 mg mL^{-1}	R 2–7	R 10–60 min	R 0.02–0.12 g		
		O 50 mg mL^{-1}	O 6	E 30 min	O 0.05 g		
	Cu^{2+}	R 50–400 mg mL^{-1}	R 2–7	R 10–60 min	R 0.02–0.12 g		
		O 50 mg mL^{-1}	O 4	E 30 min	O 0.1 g		
4-Amino-5-methyl-1,2,4-triazole-3(4H)-thion (AMTT)	Hg^{2+}		R 2–11	R 5 min-20 h	R 0.01–0.1 g	R 20, 35, 45, and 60 °C	169
			O 6	E 8 h	O 0.06 g	E 20 °C	
APTES	Cu^{2+}	R 50–500 mg mL^{-1}	R 2–12	R 0–48 h	R 0.05–1.6 g		170
		O 500 mg mL^{-1}	O 6	E 24 h	O 0.05 g		
	Ni^{2+}	R 50–500 mg mL^{-1}	R 2–12	R 0–8 h	R 0.05–1.6 g		
		O 500 mg mL^{-1}	O 6	E 5 h	O 0.05 g		
MPTMS	Hg^{2+}		R 2–7	R 0–6 h	R 0.05–1.25 mg mL^{-1}		171
			O 6	E 1 h	O 0.5 mg mL^{-1}		
	Cu^{2+}		R 2–7	R 0–6 h	R 0.2–5 mg mL^{-1}		
			O 4	E 2 h	O 2 mg mL^{-1}		
Activated carbon	Pb^{2+}	R 10–300 mg mL^{-1}	R 2–7	R 0–60 min	R 20–500 mg	R 20, 35, 45, and 60 °C	172
		O 10 mg mL^{-1}	O 6	E 30 min	O 500 mg	E 60 °C	
Iron(III)chloride hexahydrate ($FeCl_3 \cdot 6H_2O$), iron(II)chloride tetrahydrate ($FeCl_2 \cdot 4H_2O$), and chitosan (CS)	Cd^{2+}		R 3–8	R 0–600 min	R 0.005 to 0.03 g		173
			O 8	E 120 min	O 0.02 g		
Gelatin	Hg^{2+}		R 3–7	R 5–120 min			174
			O 6	E 15 min			

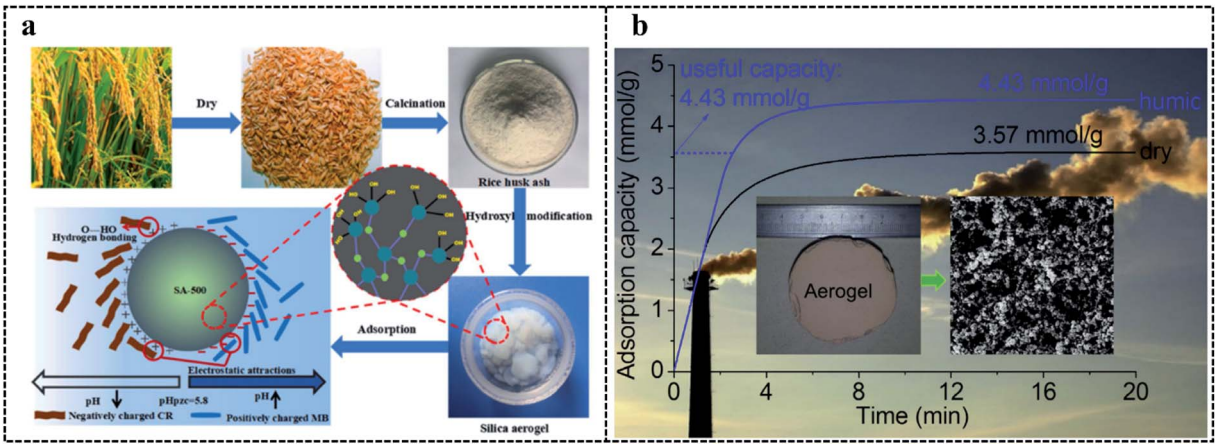

Fig. 6 (a) The adsorption of hydroxyl modified SAs for CR and MB.[187] Copyright 2021, Elsevier. (b) The adsorption of RF/SiO_2 aerogels for CO_2.[188] Copyright 2015, Elsevier.

modified SAs to adsorb oil. The TMCS, as a surface-modified silane, endowed SAs with the highest surface area value (798 $m^2\ g^{-1}$) and superhydrophobicity ($\theta = 152°$). MTMS-modified and MEMO-modified SAs had different surface area values (528 and 223 $m^2\ g^{-1}$), and their contact angle values were 142° and 120°, respectively. These characteristics lead to the adsorption capacity of TMCS-modified SAs for kerosene and diesel oil being 12.5 g g^{-1} and 11.6 g g^{-1}, while MTMS-modified SAs was 8.1 g g^{-1} and 8.7 g g^{-1}, respectively.

Excessive CO_2 emission is an important factor contributing to global warming, which means the adsorption of CO_2 is indispensable. The high porosity of SAs endows them with high adsorption ability. The high selectivity of the amino groups for CO_2 also offers the opportunity for selectively adsorption of amino-modified SAs for CO_2.[190] For example, Linneen *et al.*[191] prepared SAs which were grafted by silane with different amounts of amine units. The CO_2 adsorption ability gradually increased with the increased number of amine units. This phenomenon was caused by the absorbability of amine units for CO_2. Meanwhile, the humidity was verified to be a positive factor for CO_2 adsorption. For example, Kong *et al.*[188] prepared RF/SiO_2 aerogels, and APTES was used as a precursor to endow aerogels with amine groups (Fig. 6b). The total CO_2 adsorption ability of RF/SiO_2 aerogels at 30 °C under dry and humid 1% CO_2 was 3.57 and 4.43 mmol g^{-1}, which indicated the favorable adsorption under humid conditions. Excitedly, after 50 cyclic adsorption–desorption tests, the adsorption ability decreased from 4.43 to 4.29 mmol g^{-1} and from 3.57 to 3.51 mmol g^{-1}, under dry and humid conditions, respectively. This strong cycling stability was caused by the stability of chemically modified amine groups, different from the weak cycling stability of physically modified amine groups which was caused by the consumption of physically modified amine groups under humidity conditions. Except for humidity, temperature is another influencing factor for CO_2 adsorption. For example, Zhao *et al.*[192] prepared tetraethylenepentamine-functionalized silica foam. When the temperature increased from 30 °C to 75 °C, the CO_2 adsorption ability gradually increased to 4.75 mmol g^{-1}, which was caused by the improved CO_2 diffusion with the increase of temperature. However, the CO_2 adsorption ability gradually decreased with the increase of temperature from 75 °C to 105 °C, which is due to the fact that the reaction between CO_2 and amine groups was exothermic. Thus, the adsorption was transformed into thermodynamic control when the temperature exceeded 75 °C, indicating that the high temperature was adverse to adsorption. In addition to amino-modified SAs, SAs loading sorbents such as K_2CO_3 also showed high CO_2 adsorption performance. For example, Guo *et al.*[193] impregnated silica wet gels in K_2CO_3 ethanol solution to obtain K_2CO_3 loaded SAs and the CO_2 adsorption measurement was conducted under the 1% CO_2 and 2% H_2O at 20 °C. The maximum CO_2 capture ability and K_2CO_3 utilization efficiency achieve 1.32 mmol CO_2/g and 88.62% at 20 wt% K_2CO_3, respectively.

5.3 Cherenkov detector radiator

The yellow cluster in the keywords network shows the application for Cherenkov detector radiator. The frequent keywords in this cluster are Cherenkov radiator, RICH (ring imaging Cherenkov), BELLE, and particle identification, which shows that they are installed on Cherenkov detector as Cherenkov detector radiators to achieve particle identification. When the movement velocity of a charged particle in a medium is faster than the speed of light in this medium, Cherenkov radiation can be produced.[194] Thus, particle identification can be achieved by measuring their velocity and momentum according to Cherenkov radiation.[195] SAs were used as radiators by virtue of their low refractive index and high transparency. At present, they have been applied in threshold Cherenkov counters and RICH counters.[196,197] These two kinds of Cherenkov counters identified particles in different forms: one showed particles that exceeded the threshold,[198] the other distinguished particles by the position of the circular image.[199] For example, Adachi *et al.*[200] utilized a threshold Cherenkov counter equipped with silica aerogels to identify π and K. Owing to the low refractive index (1.013) of silica aerogels, identifying particles whose

momentum in the 1.0–2.5 GeV/c range was adequate. The high transparency of silica aerogels can compensate for low photon yield by increasing thickness. After the diffuse scattering system collected light and fine-mesh type photomultipliers improved the viability of readout, the distinguish efficiency of π and K was greater than 90%. Similarly, Bellunato *et al.*[201] utilized a RICH detector equipped with silica aerogels whose refractive index were 1.0306 and 1.0298 to identify π and P. The test results showed that π and P were distinguished when the momentum was in the 6–10 GeV/c range.

5.4 Other applications

In addition to the above-mentioned applications from the keyword network, SAs are also widely used in other fields, such as catalyst carriers, drug delivery, and optical devices.

SAs have the characteristics of high specific surface area and high porosity, which endows them as catalyst carriers.[202–204] Compared with catalysts alone, catalysts loaded on SAs not only improved stability but also are easier to facile recovery and reuse.[205,206] For example, Lisboa *et al.*[207] loaded lipase onto SAs. After incubation at 40 °C for 6 days, free lipase was inactivated, while the activity of lipase loaded on SAs was more than 50%. The conversion rate reached 70% when they were placed in an organic medium for 144 h at 40 °C. Meanwhile, because the biocompatibility of silica particles has been widely researched and has shown high biocompatibility, SAs are also used for drug delivery.[208,209] SAs can load drugs with low water solubility to improve drug delivery at the site.[210–212] For example, Smirnova *et al.*[213] loaded the low soluble drugs, such as ketoprofen and griseofulvin, onto hydrophilic silica aerogels by supercritical CO_2. Owing to the collapse of hydrophilic aerogels in liquids, the dissolution rate of drugs is quickly enhanced in liquids, which improves the bioavailability of low soluble drugs. In addition, with the low refractive index and high transparency, SAs have been introduced into the optical fiber[214,215] and laser glass.[216]

6. Conclusions

So far, SAs have been applied extensively in many fields. With the assistance of bibliometric analysis, we identify and analyze research hotspots including SA synthesis, mechanical property regulation, and their applications for thermal insulation, adsorption, and Cherenkov detector radiators. According to different synthesis technologies for different shapes, SAs are divided into three categories: PSAs, FSAs, and 3D printing SAs. Because the PSAs are composed of necklace-like silica particles through the sol–gel process. The connection points between silica are weak. It means that PSAs are easy to crack in the subsequent processing and use, which limits their applications. After the introduction of freeze casting and spinning technologies, stacked fibers accumulate into PSAs. The transformation of major pores and the densification of minor pores endow FSAs with a stronger compressible ability. It means that FSAs have good processibility. Recently, 3D printing technology is used to produce 3D printing SAs. 3D printing SAs are manufactured in the desired shape, which decreases subsequent processing and the possibility of cracking. Thus, to improve their processibility, some strategies are adopted to improve mechanical properties including prolonging aging time, cross-linking, and adding reinforcing phases. Next, we discuss the application of SAs for thermal insulation, adsorption, and Cherenkov detector radiator. Owing to their low density and porosity, SAs have the potential to be thermal insulation materials. Meanwhile, the thermal conductivity can be further decreased by regulating the structure, reducing the pore size, and adding opacifiers with high infrared radiation scattering or absorption ability. Easily modified structure and a mass of adsorption sites brought by large surface areas endow them with adsorption ability. Their adsorption ability is applied in adsorption for heavy metal ions, oil, organic dyes, and CO_2. They can also be applied as Cherenkov detector radiators. However, despite the extensive study of SAs, there are still many challenges and opportunities in the future as follows.

(1) Eco-friendly synthesis is critical to environmental pollution and the health of operators. Thus, in the process of preparation for SAs, how to use green and pollution-free reagents to obtain SAs needs to be considered. It is worth noting that the burning of rice paddy generates a mass of rice husk ash every year. In recent years, rice husk ash, as a non-toxic silicon source, is used as a precursor to producing SAs.[217,218] However, the solvent in the synthesis and aging process is usually poisonous and volatile, which results in serious environmental pollution. How to design a synthetic method, using a non-toxic solvent in the process of synthesis and aging, is need to be further explored.

(2) In processing and real applications, SAs could be subjected to a variety of stresses. However, many studies focused on the enhancement of hardness and compressibility performance. Other bearing conditions, such as twist and bend, are not discussed. Thus, other bearing conditions of SAs should be measured and improved to meet different work situations.

(3) With the development of 3D printing, we can manufacture structurally different products. However, computer techniques such as simulation have not been applied to design the structure of SAs. For example, the finite element method was used to simulate the total deformation ability of products with different structures.[219] According to the deformation and stress distribution region obtained by the simulation, we can determine the structure with the best mechanical properties and deformation ability. It means that using these techniques, we can design the structure with better capability (such as compression performance and thermal insulation) to meet different needs.

(4) 3D printing technology can directly produce 3D printing objects from a computer-aided design model, which endows them with potential for mass manufacturing. However, 3D printing objects need to be solidified to maintain an original shape after 3D printing, and the research on the solidification methods is not enough. From the perspective of large-scale preparation of SAs, thermal solidification is an effective solidification method. In addition to this, freeze casting is a feasible method to produce other aerogels though it has been not used

to produce 3D printing SAs. Combining freeze casting and a more intelligent temperature control system has the potential to become a scale production method. Meanwhile, freeze casting allows Newtonian fluid as ink, which enlarges the variety of inks.

Author contributions

Chao Ji: Methodology, Data curation, Formal analysis, Software, Visualization, Writing - original draft. Shuang Zhu: Methodology, Software, Formal analysis, Writing - review & editing. Enshuang Zhang: Methodology, Data Curation, Writing – review & editing. Wenjing Li: Methodology, Writing – review & editing. Yuanyuan Liu: Methodology, Writing – review & editing. Wanlin Zhang: Writing – review & editing. Chunjian Su: Methodology, Writing – review & draft, Supervision. Zhanjun Gu: Methodology, Writing – review & draft, Supervision, Funding acquisition. Hao Zhang: Resources, Writing – review & draft, Supervision, Funding acquisition.

Conflicts of interest

"There are no conflicts to declare".

Acknowledgements

This work was supported by Strategic Priority Research Program of Chinese Academy of Sciences [XDB36000000]; National Basic Research Program of China [2020YFA0710702 and 2021YFA1201200]; National Natural Science Foundation of China [52075510]; Directional Institutionalized Scientific Research Platform relies on Beijing Synchrotron Radiation Facility of Chinese Academy of Sciences; and Beijing Natural Science Foundation [2222087].

Notes and references

1 D. W. Schaefer and K. D. Keefer, *Phys. Rev. Lett.*, 1986, **56**, 2199–2202.
2 I. Smirnova and P. Gurikov, *J. Supercrit. Fluids*, 2018, **134**, 228–233.
3 L. Cao, Y. Si, X. Yin, J. Yu and B. Ding, *ACS Appl. Mater. Interfaces*, 2019, **11**, 35333–35342.
4 C. Wang, X. Chen, B. Wang, M. Huang, B. Wang, Y. Jiang and R. S. Ruoff, *ACS Nano*, 2018, **12**, 5816–5825.
5 P. Yan, E. Brown, Q. Su, J. Li, J. Wang, C. Xu, C. Zhou and D. Lin, *Small*, 2017, **13**, 1701756.
6 N. Hüsing and U. Schubert, *Angew. Chem., Int. Ed.*, 1998, **37**, 22–45.
7 M. Reim, W. Körner, J. Manara, S. Korder, M. Arduini-Schuster, H.-P. Ebert and J. Fricke, *Sol. Energy*, 2005, **79**, 131–139.
8 B. E. Yoldas, M. J. Annen and J. Bostaph, *Chem. Mater.*, 2000, **12**, 2475–2484.
9 E. Zhang, W. Zhang, T. lv, J. Li, J. Dai, F. Zhang, Y. Zhao, J. Yang, W. Li and H. Zhang, *ACS Appl. Mater. Interfaces*, 2021, **13**, 20548–20558.
10 E. Hu, X. Wu, S. Shang, X.-m. Tao, S.-x. Jiang and L. Gan, *J. Cleaner Prod.*, 2016, **112**, 4710–4718.
11 X. Ye, S. Shang, Y. Zhao, S. Cui, Y. Zhong and L. Huang, *Cellulose*, 2021, **28**, 7201–7212.
12 S. Takeshita, S. Akasaka and S. Yoda, *Mater. Lett.*, 2019, **254**, 258–261.
13 K. Wu, W. Dong, Y. Pan, J. Cao, Y. Zhang and D. Long, *Ind. Eng. Chem. Res.*, 2021, **60**, 1241–1249.
14 C. A. García-González, M. Jin, J. Gerth, C. Alvarez-Lorenzo and I. Smirnova, *Carbohydr. Polym.*, 2015, **117**, 797–806.
15 J. Zhao, C. Lu, X. He, X. Zhang, W. Zhang and X. Zhang, *ACS Appl. Mater. Interfaces*, 2015, **7**, 2607–2615.
16 S. Zhao, W. J. Malfait, N. Guerrero-Alburquerque, M. M. Koebel and G. Nyström, *Angew. Chem., Int. Ed.*, 2018, **57**, 7580–7608.
17 S. D. Bhagat and A. V. Rao, *Appl. Surf. Sci.*, 2006, **252**, 4289–4297.
18 M. A. Cauqui and J. M. Rodríguez-Izquierdo, *J. Non-Cryst. Solids*, 1992, **147–148**, 724–738.
19 S. S. Kistler, *Nature*, 1931, **127**, 741.
20 S. D. Bhagat, Y.-H. Kim, K.-H. Suh, Y.-S. Ahn, J.-G. Yeo and J.-H. Han, *Microporous Mesoporous Mater.*, 2008, **112**, 504–509.
21 Y. Si, J. Yu, X. Tang, J. Ge and B. Ding, *Nat. Commun.*, 2014, **5**, 5802.
22 C. Jia, L. Li, Y. Liu, B. Fang, H. Ding, J. Song, Y. Liu, K. Xiang, S. Lin, Z. Li, W. Si, B. Li, X. Sheng, D. Wang, X. Wei and H. Wu, *Nat. Commun.*, 2020, **11**, 3732.
23 L. Su, H. Wang, M. Niu, S. Dai, Z. Cai, B. Yang, H. Huyan and X. Pan, *Sci. Adv.*, 2020, **6**, eaay6689.
24 J. Yang, H. Wang, B. Zhou, J. Shen, Z. Zhang and A. Du, *Langmuir*, 2021, **37**, 2129–2139.
25 S. Zhao, G. Siqueira, S. D Rdova, D. Norris and W. J. Malfait, *Nature*, 2020, **584**, 387–392.
26 N. Karamat-Ullah, Y. Demidov, M. Schramm, D. Grumme, J. Auer, C. Bohr, B. Brachvogel and H. Maleki, *ACS Biomater. Sci. Eng.*, 2021, **7**, 4545–4556.
27 J. J. Moyano, J. Loizillon, D. Pérez-Coll, M. Belmonte, P. Miranzo, D. Grosso and M. I. Osendi, *J. Eur. Ceram. Soc.*, 2021, **41**, 2908–2917.
28 A. Du, H. Wang, B. Zhou, C. Zhang, X. Wu, Y. Ge, T. Niu, X. Ji, T. Zhang, Z. Zhang, G. Wu and J. Shen, *Chem. Mater.*, 2018, **30**, 6849–6857.
29 P. Hu, L. Liu, M. Zhao, J. Wang, X. Ma and J. Wang, *ES Mater. Manuf.*, 2021, **15**, 14–33.
30 T. Huang, Y. Zhu, J. Zhu, H. Yu, Q. Zhang and M. Zhu, *Adv. Fiber Mater.*, 2020, **2**, 338–347.
31 P. B. Sarawade, J.-K. Kim, A. Hilonga and H. T. Kim, *Solid State Sci.*, 2010, **12**, 911–918.
32 S. Yun, T. Guo, J. Zhang, L. He, Y. Li, H. Li, X. Zhu and Y. Gao, *J. Sol-Gel Sci. Technol.*, 2017, **83**, 53–63.
33 T.-Y. Wei, T.-F. Chang, S.-Y. Lu and Y.-C. Chang, *J. Am. Ceram. Soc.*, 2007, **90**, 2003–2007.
34 P. Tsou, *J. Non-Cryst. Solids*, 1995, **186**, 415–427.
35 J. Matijevic and D. Shirley, *Control Eng. Pract.*, 1997, **5**, 827–835.

36 M. Tabata, I. Adachi, H. Kawai, M. Kubo and T. Sato, *Phys. Procedia*, 2012, **37**, 642–649.
37 M. Reim, A. Beck, W. Körner, R. Petricevic, M. Glora, M. Weth, T. Schliermann, J. Fricke, C. Schmidt and F. J. Pötter, *Sol. Energy*, 2002, **72**, 21–29.
38 J. Wernery, A. Ben-Ishai, B. Binder and S. Brunner, *Energy Procedia*, 2017, **134**, 490–498.
39 H. Liu, W. Sha, A. T. Cooper and M. Fan, *Colloids Surf., A*, 2009, **347**, 38–44.
40 T. Liu, Q. Liu, Y. Liu, H. Yao, Z. Zhang, X. Wang and J. Shen, *J. Sol-Gel Sci. Technol.*, 2021, **98**, 389–400.
41 S. Štandeker, Z. Novak and Ž. Knez, *J. Colloid Interface Sci.*, 2007, **310**, 362–368.
42 Y. Yu, Q. Ma, J.-b. Zhang and G.-b. Liu, *Appl. Surf. Sci.*, 2020, **512**, 145697.
43 Y. Song, X. Chen, T. Hao, Z. Liu and Z. Lan, *Comput. Educ.*, 2019, **137**, 12–31.
44 O. Ellegaard and J. A. Wallin, *Scientometrics*, 2015, **105**, 1809–1831.
45 S. Zhu, H. Meng, Z. Gu and Y. Zhao, *Nano Today*, 2021, **39**, 101233.
46 S. Zhu, L. Li, Z. Gu, C. Chen and Y. Zhao, *Small*, 2020, **16**, 2000980.
47 J. Xie, M. Zhao, C. Wang, Y. Yong and Z. Gu, *Chem. Eng. J.*, 2022, **435**, 134976.
48 K. Ullmann, P. Ádám and K. Sinkó, *J. Non-Cryst. Solids*, 2018, **499**, 394–400.
49 C. Macías, M. Haro, J. B. Parra, G. Rasines and C. O. Ania, *Carbon*, 2013, **63**, 487–497.
50 Z. Zahedi and S. Haustein, *J. Informetr*, 2018, **12**, 191–202.
51 K. Saikia, M. Vallès, A. Fabregat, R. Saez and D. Boer, *Sol. Energy*, 2020, **199**, 100–114.
52 J. Tse, D. E. Schrader, D. Ghosh, T. Liao and D. Lundie, *Ethics Inf. Technol.*, 2015, **17**, 153–163.
53 P. Ball, *Nature*, 2005, **436**, 900.
54 A. Thor and L. Bornmann, *Online Inf. Rev.*, 2011, **35**, 291–300.
55 L. Ding, L. Chen, C. Ding and J. Tao, *Chin. Geogr. Sci.*, 2019, **29**, 1–12.
56 N. van Eck and L. Waltman, *Scientometrics*, 2010, **84**, 523–538.
57 P. B. Wagh, R. Begag, G. M. Pajonk, A. V. Rao and D. Haranath, *Mater. Chem. Phys.*, 1999, **57**, 214–218.
58 L. Wang, J. Feng, Y. Luo, Z. Zhou, Y. Jiang, X. Luo, L. Xu, L. Li and J. Feng, *ACS Appl. Mater. Interfaces*, 2021, **13**, 40964–40975.
59 J. L. Gurav, I.-K. Jung, H.-H. Park, E. S. Kang and D. Y. Nadargi, *J. Nanomater.*, 2010, **2010**, 409310.
60 Q. Liu, K. Yan, J. Chen, M. Xia, M. Li, K. Liu, D. Wang, C. Wu and Y. Xie, *Aggregate*, 2021, **2**, e30.
61 Z. Guo, R. Yang, T. Wang, L. An, S. Ren and C. Zhou, *J. Manuf. Sci. Eng.*, 2020, **143**, 011011.
62 G. Guzel Kaya and H. Deveci, *J. Ind. Eng. Chem.*, 2020, **89**, 13–27.
63 L. L. Hench and J. K. West, *Chem. Rev.*, 1990, **90**, 33–72.
64 H. Tamon, T. Kitamura and M. Okazaki, *J. Colloid Interface Sci.*, 1998, **197**, 353–359.
65 H. Maleki, L. Durães and A. Portugal, *J. Non-Cryst. Solids*, 2014, **385**, 55–74.
66 Z. Shao, F. Luo, X. Cheng and Y. Zhang, *Mater. Chem. Phys.*, 2013, **141**, 570–575.
67 C. J. Lee, G. S. Kim and S. H. Hyun, *J. Mater. Sci.*, 2002, **37**, 2237–2241.
68 D. Y. Nadargi and A. V. Rao, *J. Alloys Compd.*, 2009, **467**, 397–404.
69 A. Venkateswara Rao, S. D. Bhagat, H. Hirashima and G. M. Pajonk, *J. Colloid Interface Sci.*, 2006, **300**, 279–285.
70 Z. Yang, H. Yu, X. Li, H. Ding and H. Ji, *J. Non-Cryst. Solids*, 2019, **525**, 119677.
71 K.-Y. Lee, D. B. Mahadik, V. G. Parale and H.-H. Park, *J. Korean Ceram. Soc.*, 2019, **57**, 1–23.
72 K. Sinkó, *Materials*, 2010, **3**, 704–740.
73 A. Venkateswara Rao, G. M. Pajonk and N. N. Parvathy, *J. Mater. Sci.*, 1994, **29**, 1807–1817.
74 C. J. Brinker, *J. Non-Cryst. Solids*, 1988, **100**, 31–50.
75 R. Ciriminna, A. Fidalgo, V. Pandarus, F. Béland, L. M. Ilharco and M. Pagliaro, *Chem. Rev.*, 2013, **113**, 6592–6620.
76 K. Nawaz, S. J. Schmidt and A. M. Jacobi, *Int. J. Heat Mass Transfer*, 2014, **74**, 25–34.
77 A. Buckley and M. Greenblatt, *J. Chem. Educ.*, 1994, **71**, 599.
78 D. Y. Nadargi, S. S. Latthe and A. Venkateswara Rao, *J. Sol-Gel Sci. Technol.*, 2009, **49**, 53–59.
79 R. A. Strøm, Y. Masmoudi, A. Rigacci, G. Petermann, L. Gullberg, B. Chevalier and M. A. Einarsrud, *J. Sol-Gel Sci. Technol.*, 2007, **41**, 291–298.
80 S. Smitha, P. Shajesh, P. R. Aravind, S. R. Kumar, P. K. Pillai and K. G. K. Warrier, *Microporous Mesoporous Mater.*, 2006, **91**, 286–292.
81 S. Hæreid, M. Dahle, S. Lima and M. A. Einarsrud, *J. Non-Cryst. Solids*, 1995, **186**, 96–103.
82 M.-A. Einarsrud, M. Britt Kirkedelen, E. Nilsen, K. Mortensen and J. Samseth, *J. Non-Cryst. Solids*, 1998, **231**, 10–16.
83 H. Omranpour, A. Dourbash and S. Motahari, *AIP Conf. Proc.*, 2014, **1593**, 298–302.
84 H. Omranpour and S. Motahari, *J. Non-Cryst. Solids*, 2013, **379**, 7–11.
85 A. Pons, L. Casas, E. Estop, E. Molins, K. D. M. Harris and M. Xu, *J. Non-Cryst. Solids*, 2012, **358**, 461–469.
86 W. P. Lee and A. F. Routh, *Langmuir*, 2004, **20**, 9885–9888.
87 S. He, D. Huang, H. Bi, Z. Li, H. Yang and X. Cheng, *J. Non-Cryst. Solids*, 2015, **410**, 58–64.
88 H. Maleki, L. Durães and A. Portugal, *J. Phys. Chem. C*, 2015, **119**, 7689–7703.
89 S. S. Çok and N. Gizli, *Ceram. Int.*, 2020, **46**, 27789–27799.
90 S.-W. Liu, Q. Wei, S.-P. Cui, Z.-R. Nie, M.-H. Du and Q.-Y. Li, *J. Sol-Gel Sci. Technol.*, 2016, **78**, 60–67.
91 M. V. Khedkar, S. B. Somvanshi, A. V. Humbe and K. M. Jadhav, *J. Non-Cryst. Solids*, 2019, **511**, 140–146.
92 T. Li, A. Du, T. Zhang, W. Ding, M. Liu, J. Shen, Z. Zhang and B. Zhou, *RSC Adv.*, 2018, **8**, 17967–17975.
93 D. Sivaraman, S. Zhao, S. Iswar, M. Lattuada and W. J. Malfait, *Adv. Eng. Mater.*, 2021, **23**, 2100376.

94 A. Venkateswara Rao, A. Parvathy Rao and M. M. Kulkarni, *J. Non-Cryst. Solids*, 2004, **350**, 224–229.
95 C. Ratti, *J. Food Eng.*, 2001, **49**, 311–319.
96 W. Abdelwahed, G. Degobert, S. Stainmesse and H. Fessi, *Adv. Drug Delivery Rev.*, 2006, **58**, 1688–1713.
97 C. Gallé, *Cem. Concr. Res.*, 2001, **31**, 1467–1477.
98 G. W. Scherer, *J. Non-Cryst. Solids*, 1993, **155**, 1–25.
99 L. T. Canham, A. G. Cullis, C. Pickering, O. D. Dosser, T. I. Cox and T. P. Lynch, *Nature*, 1994, **368**, 133–135.
100 Z. Zhang and G. W. Scherer, *Cem. Concr. Res.*, 2017, **99**, 137–154.
101 G. Guzel Kaya, E. Yilmaz and H. Deveci, *Adv. Powder Technol.*, 2020, **31**, 926–936.
102 Q. Fu, Y. Si, C. Duan, Z. Yan, L. Liu, J. Yu and B. Ding, *Adv. Funct. Mater.*, 2019, **29**, 1808234.
103 M. Dilamian, M. Joghataei, Z. Ashrafi, C. Bohr, S. Mathur and H. Maleki, *Appl. Mater. Today*, 2021, **22**, 100964.
104 T. Pirzada, Z. Ashrafi, W. Xie and S. A. Khan, *Adv. Funct. Mater.*, 2020, **30**, 1907359.
105 C. Ferraro, E. Garcia-Tuñon, V. G. Rocha, S. Barg, M. D. Fariñas, T. E. G. Alvarez-Arenas, G. Sernicola, F. Giuliani and E. Saiz, *Adv. Funct. Mater.*, 2016, **26**, 1636–1645.
106 G. Shao, D. A. H. Hanaor, X. Shen and A. Gurlo, *Adv. Mater.*, 2020, **32**, 1907176.
107 S. A. Barr and E. Luijten, *Acta Mater.*, 2010, **58**, 709–715.
108 S. Deville, *Adv. Eng. Mater.*, 2008, **10**, 155–169.
109 N. Arai, T. Stan, S. Macfarland, P. W. Voorhees, N. S. Muyanja, A. J. Shahani and K. T. Faber, *Acta Mater.*, 2021, **215**, 117039.
110 M. C. Gutiérrez, Z. Y. García-Carvajal, M. Jobbágy, F. Rubio, L. Yuste, F. Rojo, M. L. Ferrer and F. del Monte, *Adv. Funct. Mater.*, 2007, **17**, 3505–3513.
111 K. H. Zuo, Y.-P. Zeng and D. Jiang, *Mater. Sci. Eng., C*, 2010, **30**, 283–287.
112 C. M. Pekor, P. Kisa and I. Nettleship, *J. Am. Ceram. Soc.*, 2008, **91**, 3185–3190.
113 X. Li, D. Yao, K. Zuo, Y. Xia, J. Yin, H. Liang and Y.-P. Zeng, *J. Eur. Ceram. Soc.*, 2020, **40**, 5845–5851.
114 L. Xian, Y. Zhang, Y. Wu, X. Zhang, X. Dong, J. Liu and A. Guo, *Ceram. Int.*, 2020, **46**, 1869–1875.
115 M. Sun, S. Yang, X. Gao, P. Man, J. Qu, W. Zhang, S. Yin and L. Cheng, *Ceram. Int.*, 2021, **47**, 8169–8174.
116 J. Halloran, *Science*, 2006, **311**, 479–480.
117 M.-A. Shahbazi, M. Ghalkhani and H. Maleki, *Adv. Eng. Mater.*, 2020, **22**, 2000033.
118 S. Deville, E. Saiz and A. P. Tomsia, *Biomaterials*, 2006, **27**, 5480–5489.
119 K. Araki and J. W. Halloran, *J. Am. Ceram. Soc.*, 2004, **87**, 2014–2019.
120 Y. Si, X. Wang, L. Dou, J. Yu and B. Ding, *Sci. Adv.*, 2018, **4**, eaas8925.
121 F. Wang, L. Dou, J. Dai, Y. Li, L. Huang, Y. Si, J. Yu and B. Ding, *Angew. Chem., Int. Ed.*, 2020, **59**, 8285–8292.
122 L. Qiu, J. Z. Liu, S. L. Y. Chang, Y. Wu and D. Li, *Nat. Commun.*, 2012, **3**, 1241.
123 D. J. Sypeck and H. N. G. Wadley, *Adv. Eng. Mater.*, 2002, **4**, 759–764.
124 L. Dou, X. Zhang, X. Cheng, Z. Ma, X. Wang, Y. Si, J. Yu and B. Ding, *ACS Appl. Mater. Interfaces*, 2019, **11**, 29056–29064.
125 X. Xu, Q. Zhang, M. Hao, Y. Hu, Z. Lin, L. Peng, T. Wang, X. Ren, C. Wang, Z. Zhao, C. Wan, H. Fei, L. Wang, J. Zhu, H. Sun, W. Chen, T. Du, B. Deng, J. Cheng Gary, I. Shakir, C. Dames, S. Fisher Timothy, X. Zhang, H. Li, Y. Huang and X. Duan, *Science*, 2019, **363**, 723–727.
126 T. M. Tillotson and L. W. Hrubesh, *J. Non-Cryst. Solids*, 1992, **145**, 44–50.
127 H. Wang, X. Zhang, N. Wang, Y. Li, X. Feng, Y. Huang, C. Zhao, Z. Liu, M. Fang, G. Ou, H. Gao, X. Li and H. Wu, *Sci. Adv.*, 2017, **3**, e1603170.
128 T. Tian, T.-W. Zhang, Y.-C. Yin, Y.-H. Tan, Y.-H. Song, L.-L. Lu and H.-B. Yao, *Nano Lett.*, 2019, **20**, 677–685.
129 J. A. Lewis, *Adv. Funct. Mater.*, 2006, **16**, 2193–2204.
130 V. C.-F. Li, C. K. Dunn, Z. Zhang, Y. Deng and H. J. Qi, *Sci. Rep.*, 2017, **7**, 8018.
131 Z. Guo, R. Yang, T. Wang, L. An, S. Ren and C. Zhou, *J. Manuf. Sci. Eng.*, 2021, **143**, 011011.
132 B. S. Chava, E. K. Thorn and S. Das, *Phys. Chem. Chem. Phys.*, 2021, **23**, 24634–24645.
133 A. Shahzad and I. Lazoglu, *Composites, Part B*, 2021, **225**, 109249.
134 D. Kam, M. Chasnitsky, C. Nowogrodski, I. Braslavsky, T. Abitbol, S. Magdassi and O. Shoseyov, *Colloids Interfaces*, 2019, **3**, 46.
135 H. Tetik, Y. Wang, X. Sun, D. Cao, N. Shah, H. Zhu, F. Qian and D. Lin, *Adv. Funct. Mater.*, 2021, **31**, 2103410.
136 J. Ma, F. Ye, C. Yang, J. Ding, S. Lin, B. Zhang and Q. Liu, *Mater. Des.*, 2017, **131**, 226–231.
137 N. Leventis, C. Sotiriou-Leventis, G. Zhang and A.-M. M. Rawashdeh, *Nano Lett.*, 2002, **2**, 957–960.
138 R. Liu, X. Dong, S. Xie, T. Jia, Y. Xue, J. Liu, W. Jing and A. Guo, *Chem. Eng. J.*, 2019, **360**, 464–472.
139 S. Karamikamkar, H. E. Naguib and C. B. Park, *Adv. Colloid Interface Sci.*, 2020, **276**, 102101.
140 L. Jiang, K. Kato, K. Mayumi, H. Yokoyama and K. Ito, *ACS Macro Lett.*, 2017, **6**, 281–286.
141 M. A. B. Meador, E. F. Fabrizio, F. Ilhan, A. Dass, G. Zhang, P. Vassilaras, J. C. Johnston and N. Leventis, *Chem. Mater.*, 2005, **17**, 1085–1098.
142 S. P. Patil, P. Shendye and B. Markert, *Composites, Part B*, 2020, **190**, 107884.
143 A. Lamy-Mendes, W. J. Malfait, A. Sadeghpour, A. V. Girão, R. F. Silva and L. Durães, *Carbon*, 2021, **180**, 146–162.
144 A. Ślosarczyk, *Nanomaterials*, 2017, **7**, 44.
145 J. He, H. Zhao, X. Li, D. Su, F. Zhang, H. Ji and R. Liu, *J. Hazard. Mater.*, 2018, **346**, 199–207.
146 G. Wei, Y. Liu, X. Zhang, F. Yu and X. Du, *Int. J. Heat Mass Transfer*, 2011, **54**, 2355–2366.
147 J. Fricke, X. Lu, P. Wang, D. Büttner and U. Heinemann, *Int. J. Heat Mass Transfer*, 1992, **35**, 2305–2309.
148 J. Fricke and T. Tillotson, *Thin Solid Films*, 1997, **297**, 212–223.

149 N. Bheekhun, A. R. Abu Talib and M. R. Hassan, *Adv. Mater. Sci. Eng.*, 2013, **2013**, 1–18.
150 V. P. Carey, G. Chen, C. Grigoropoulos, M. Kaviany and A. Majumdar, *Nanoscale Microscale Thermophys. Eng.*, 2008, **12**, 1–60.
151 D. Bi, H. Chen and T. Ye, *Cryogenics*, 2012, **52**, 403–409.
152 A. J. H. McGaughey and M. Kaviany, *Int. J. Heat Mass Transfer*, 2004, **47**, 1799–1816.
153 R. Prasher, *Nano Lett.*, 2005, **5**, 2155–2159.
154 Y. Lei, Z. Hu, B. Cao, X. Chen and H. Song, *Mater. Chem. Phys.*, 2017, **187**, 183–190.
155 Z. Deng, J. Wang, A. Wu, J. Shen and B. Zhou, *J. Non-Cryst. Solids*, 1998, **225**, 101–104.
156 V. Apostolopoulou-Kalkavoura, P. Munier and L. Bergström, *Adv. Mater.*, 2021, **33**, 2001839.
157 Y. Lei, X. Chen, Z. Hu, H. Song and B. Cao, *Scr. Mater.*, 2017, **139**, 5–8.
158 L. Dou, X. Cheng, X. Zhang, Y. Si, J. Yu and B. Ding, *J. Mater. Chem. A*, 2020, **8**, 7775–7783.
159 S. Liu, X. Wu, Y. Li, S. Cui, X. Shen and G. Tan, *Appl. Therm. Eng.*, 2021, **190**, 116745.
160 L. Shang, Y. Lyu and W. Han, *Materials*, 2019, **12**, 993.
161 H. Zhang, W.-Z. Fang, X. Wang, Y.-M. Li and W.-Q. Tao, *Int. J. Heat Mass Transfer*, 2017, **115**, 21–31.
162 J. Zhu, H. Ren and Y. Bi, *J. Porous Mater.*, 2018, **25**, 1697–1705.
163 V. G. Parale, H.-N.-R. Jung, W. Han, K.-Y. Lee, D. B. Mahadik, H. H. Cho and H.-H. Park, *J. Alloys Compd.*, 2017, **727**, 871–878.
164 K. Rehman, F. Fatima, I. Waheed and M. S. H. Akash, *J. Cell. Biochem.*, 2018, **119**, 157–184.
165 S. Štandeker, Z. Novak and Ž. Knez, *J. Hazard. Mater.*, 2009, **165**, 1114–1118.
166 M.-H. Sun, S.-Z. Huang, L.-H. Chen, Y. Li, X.-Y. Yang, Z.-Y. Yuan and B.-L. Su, *Chem. Soc. Rev.*, 2016, **45**, 3479–3563.
167 N. Hüsing and U. Schubert, *J. Sol-Gel Sci. Technol.*, 1997, **8**, 807–812.
168 H. R. Pouretedal and M. Kazemi, *Int. J. Ind. Chem.*, 2012, **3**, 20.
169 F. Tadayon, M. Saber-Tehrani and S. Motahar, *Korean J. Chem. Eng.*, 2013, **30**, 642–648.
170 H. Faghihian, H. Nourmoradi and M. Shokouhi, *Desalin. Water Treat.*, 2013, **52**, 305–313.
171 S. Štandeker, A. Veronovski, Z. Novak and Ž. Knez, *Desalination*, 2011, **269**, 223–230.
172 T. Fariba, H. Mina and M. Shiva, *J. Chin. Chem. Soc.*, 2012, **59**, 1578–1583.
173 Z. Shariatinia and A. Esmaeilzadeh, *Water Environ. Res.*, 2019, **91**, 1624–1637.
174 P. Herman, I. Fábián and J. Kalmár, *ACS Appl. Nano Mater.*, 2020, **3**, 195–206.
175 P. K. Jal, S. Patel and B. K. Mishra, *Talanta*, 2004, **62**, 1005–1028.
176 M. Hasanpour and M. Hatami, *Adv. Colloid Interface Sci.*, 2020, **284**, 102247.
177 H. Maleki, *Chem. Eng. J.*, 2016, **300**, 98–118.
178 S. S. Mirzaee, E. Salahi and A. Khanlarkhani, *J. Dispersion Sci. Technol.*, 2019, **40**, 657–667.
179 M. Li, M.-y. Li, C.-g. Feng and Q.-x. Zeng, *Appl. Surf. Sci.*, 2014, **314**, 1063–1069.
180 S. Sertsing, T. Chukeaw, S. Pengpanich and B. Pornchuti, *MATEC Web Conf.*, 2018, **156**, 03014.
181 L. Zhang, C. Yu, W. Zhao, Z. Hua, H. Chen, L. Li and J. Shi, *J. Non-Cryst. Solids*, 2007, **353**, 4055–4061.
182 C. M. C. Filho, T. Matias, L. Durães and A. J. M. Valente, *Colloids Surf., A*, 2017, **520**, 550–560.
183 R. Tang, W. Hong, C. Srinivasakannan, X. Liu, X. Wang and X. Duan, *Sep. Purif. Technol.*, 2022, **281**, 119950.
184 J. Huang, H. Liu, S. Chen and C. Ding, *J. Environ. Chem. Eng.*, 2016, **4**, 3274–3282.
185 D. D. E. Koyuncu and M. Okur, *Colloids Surf., A*, 2021, **628**, 127370.
186 A. Abolghasemi Mahani, S. Motahari and A. Mohebbi, *Mar. Pollut. Bull.*, 2018, **129**, 438–447.
187 K. Chen, Q. Feng, D. Ma and X. Huang, *Colloids Surf., A*, 2021, **616**, 126331.
188 Y. Kong, X. Shen, S. Cui and M. Fan, *Appl. Energy*, 2015, **147**, 308–317.
189 S. Sert Çok, F. Koç and N. Gİzlİ, *J. Hazard. Mater.*, 2021, **408**, 124858.
190 C. Chen, S. Zhang, K. H. Row and W.-S. Ahn, *J. Energy Chem.*, 2017, **26**, 868–880.
191 N. N. Linneen, R. Pfeffer and Y. S. Lin, *Chem. Eng. J.*, 2014, **254**, 190–197.
192 P. Zhao, G. Zhang, Y. Xu, Y.-K. Lv, Z. Yang and H. Cheng, *Energy Fuels*, 2019, **33**, 3357–3369.
193 Y. Guo, C. Zhao, J. Sun, W. Li and P. Lu, *Fuel*, 2018, **215**, 735–743.
194 T. M. Shaffer, E. C. Pratt and J. Grimm, *Nat. Nanotechnol.*, 2017, **12**, 106–117.
195 C. Lippmann, *Nucl. Instrum. Methods Phys. Res., Sect. A*, 2012, **666**, 148–172.
196 L. Cremaldi, D. A. Sanders, P. Sonnek, D. J. Summers and J. Reidy, *IEEE Trans. Nucl. Sci.*, 2009, **56**, 1475–1478.
197 Y. N. Kharzheev, *Phys. Part. Nucl.*, 2008, **39**, 107–135.
198 C. Grupen, *AIP Conf. Proc.*, 2000, **536**, 3–34.
199 J. Seguinot and T. Ypsilantis, *Nucl. Instrum. Methods Phys. Res., Sect. A*, 1994, **343**, 1–29.
200 I. Adachi, T. Sumiyoshi, K. Hayashi, N. Iida, R. Enomoto, K. Tsukada, R. Suda, S. Matsumoto, K. Natori, M. Yokoyama and H. Yokogawa, *Nucl. Instrum. Methods Phys. Res., Sect. A*, 1995, **355**, 390–398.
201 T. Bellunato, A. Braem, A. R. Buzykaev, M. Calvi, E. Chesi, A. F. Danilyuk, S. Easo, C. Hansen, S. Jolly, C. Joram, E. A. Kravchenko, D. Liko, C. Matteuzzi, M. Musy, P. Negri, N. Neufeld, A. P. Onuchin, J. Seguinot, P. Weilhammer and S. Wotton, *Nucl. Instrum. Methods Phys. Res., Sect. A*, 2003, **502**, 227–230.
202 E. T. Hwang and M. B. Gu, *Eng. Life Sci.*, 2013, **13**, 49–61.
203 S. Paul and J. H. Clark, *Green Chem.*, 2003, **5**, 635–638.
204 M. Paljevac, M. Primožič, M. Habulin, Z. Novak and Ž. Knez, *J. Supercrit. Fluids*, 2007, **43**, 74–80.
205 A. Wolny and A. Chrobok, *Nanomaterials*, 2021, **11**, 2030.

206 T. Jesionowski, J. Zdarta and B. Krajewska, *Adsorption*, 2014, **20**, 801–821.
207 M. C. Lisboa, C. A. Rodrigues, A. S. Barbosa, S. Mattedi, L. S. Freitas, A. A. Mendes, C. Dariva, E. Franceschi, Á. Lima and C. M. F. Soares, *Process Biochem.*, 2018, **75**, 157–165.
208 P. Veres, M. Kéri, I. Bányai, I. Lázár, I. Fábián, C. Domingo and J. Kalmár, *Colloids Surf., B*, 2017, **152**, 229–237.
209 J. Stergar and U. Maver, *J. Sol-Gel Sci. Technol.*, 2016, **77**, 738–752.
210 H. Maleki, L. Durães, C. A. García-González, P. del Gaudio, A. Portugal and M. Mahmoudi, *Adv. Colloid Interface Sci.*, 2016, **236**, 1–27.
211 N. Ganonyan, G. Bar, R. Gvishi and D. Avnir, *RSC Adv*, 2021, **11**, 7824–7838.
212 D. D. Lovskaya, A. E. Lebedev and N. V. Menshutina, *J. Supercrit. Fluids*, 2015, **106**, 115–121.
213 I. Smirnova, S. Suttiruengwong, M. Seiler and W. Arlt, *Pharm. Dev. Technol.*, 2005, **9**, 443–452.
214 L. W. Hrubesh, *J. Non-Cryst. Solids*, 1998, **225**, 335–342.
215 L. Xiao, M. D. W. Grogan, W. J. Wadsworth, R. England and T. A. Birks, *Opt. Express*, 2011, **19**, 764–769.
216 T. M. Tillotson, W. E. Sunderland, I. M. Thomas and L. W. Hrubesh, *J. Sol-Gel Sci. Technol.*, 1994, **1**, 241–249.
217 J. P. Nayak and J. Bera, *Trans. Indian Ceram. Soc.*, 2009, **68**, 91–94.
218 A. Tadjarodi, M. Haghverdi and V. Mohammadi, *Mater. Res. Bull.*, 2012, **47**, 2584–2589.
219 S. Ma, H. Yang, S. Zhao, P. He, Z. Zhang, X. Duan, Z. Yang, D. Jia and Y. Zhou, *Composites, Part B*, 2021, **226**, 109348.